Biochimica et Biophysica Acta 1818 (2012) 135–145

Contents lists available at SciVerse ScienceDirect

Biochimica et Biophysica Acta

journal homepage: www.elsevier.com/locate/bbamem

The role of membrane thickness in charged protein–lipid interactions ☆

Libo B. Li [a], Igor Vorobyov [a], Toby W. Allen [a,b,*]

[a] Department of Chemistry, University of California, Davis. One Shields Avenue, Davis, CA, 95616, USA
[b] Health Innovations Research Institute and School of Applied Sciences, RMIT University, GPO Box 2476V, Melbourne, Victoria 3001, Australia

ARTICLE INFO

Article history:
Received 19 July 2011
Received in revised form 23 October 2011
Accepted 24 October 2011
Available online 28 October 2011

Keywords:
Protein–lipid interaction
Arginine
Ion-induced defect
Membrane thickness
Ion permeation

ABSTRACT

Charged amino acids are known to be important in controlling the actions of integral and peripheral membrane proteins and cell disrupting peptides. Atomistic molecular dynamics studies have shed much light on the mechanisms of membrane binding and translocation of charged protein groups, yet the impact of the full diversity of membrane physico-chemical properties and topologies has yet to be explored. Here we have performed a systematic study of an arginine (Arg) side chain analog moving across saturated phosphatidylcholine (PC) bilayers of variable hydrocarbon tail length from 10 to 18 carbons. For all bilayers we observe similar ion-induced defects, where Arg draws water molecules and lipid head groups into the bilayers to avoid large dehydration energy costs. The free energy profiles all exhibit sharp climbs with increasing penetration into the hydrocarbon core, with predictable shifts between bilayers of different thickness, leading to barrier reduction from 26 kcal/mol for 18 carbons to 6 kcal/mol for 10 carbons. For lipids of 10 and 12 carbons we observe narrow transmembrane pores and corresponding plateaus in the free energy profiles. Allowing for movements of the protein and side chain snorkeling, we argue that the energetic cost for burying Arg inside a thin bilayer will be small, consistent with recent experiments, also leading to a dramatic reduction in pK_a shifts for Arg. We provide evidence that Arg translocation occurs via an ion-induced defect mechanism, except in thick bilayers (of at least 18 carbons) where solubility-diffusion becomes energetically favored. Our findings shed light on the mechanisms of ion movement through membranes of varying composition, with implications for a range of charged protein–lipid interactions and the actions of cell-perturbing peptides. This article is part of a Special Issue entitled: Membrane protein structure and function.

1. Introduction

Biological membranes are both home to a range of proteins with critical functions, and protective shells that effectively block uncatalyzed permeation of polar and charged molecules. This view has prevailed for many decades and is understood in terms of the energetics of ion translocation across an oily membrane slab. However, recent studies have suggested that cell membranes may not be so impenetrable [1–3]. Given that charged protein groups, such as arginine (Arg) and lysine (Lys), can play central roles in protein structure and function (e.g. [4–10]) and the actions of a range of cell-perturbing peptides (e.g. [11–17]), this highlights the need to understand the interactions of charged protein groups with biological membranes at the molecular level.

Biological membranes are often pictured as bilayers of lipid molecules that form sheet-like non-polar regions. This rigid slab model presents large barriers to charged molecules (of several tens of kcal/mol [18]), which must dehydrate as they cross the membrane interface. This view has been challenged recently by the so called 'paddle model' of voltage gated ion channel activation, which suggested lipid-exposed movement of several charged Arg residues across the lipid membrane [1]. It was also questioned when cell biology experiments, using the translocon machinery of membrane protein synthesis, reported small (2–3 kcal/mol) energetic costs to incorporate Arg in the middle of a transmembrane protein segment [2]. More recently, a similar cost of just ~4 kcal/mol has been suggested for incorporating Arg on a host β-barrel protein (OmpLA) near the middle of a 12-carbon dilauroyl-PC (DLPC) membrane [3]. This apparent contrast between theory and experiments has sparked intense debate into the interpretation of these observations, and has led to a series of studies that have provided new understanding of the electromechanical behavior of lipid membranes.

In the absence of molecular level descriptions of membrane charge transport processes, the simplified continuum description of membranes remained unchanged for nearly half a century. However, all-atom molecular dynamics (MD) studies have revealed some largely unexpected (yet envisioned by A. Parsegian over 40 years ago [19]) physico-chemical behavior associated with the deformability of the lipid bilayer. It has since been revealed that water and lipid head groups are pulled into the non-polar membrane core due to the presence of

☆ This article is part of a Special Issue entitled: Membrane protein structure and function.

* Corresponding author at: Department of Chemistry, University of California, Davis. One Shields Avenue, Davis, CA, 95616, USA. Tel.: +1 530 754 5968; fax: +1 530 752 8995.
E-mail address: tallen@chem.ucdavis.edu (T.W. Allen).

0005-2736/$ – see front matter © 2011 Elsevier B.V. All rights reserved.
doi:10.1016/j.bbamem.2011.10.026

charged molecules (e.g. [20–24], and Fig. 1). The resulting free energy profile (or potential of mean force, PMF) for charge translocation is very different to previous continuum models, owing to the fact that the molecule never fully dehydrates, but must pay a price of deforming the membrane [21,25]. This surprising outcome has some serious consequences, including an insensitivity of translocation energetics to the chemical identify of the charged molecule or protein group (Vorobyov et al., in preparation), the binding of a counter-ion of anionic lipid head group [26], and even the dipole potential of the membrane [25]. These observations have significant implications for biological processes involving charge–membrane interactions, and have set the stage for a new level of understanding of membrane transport processes.

All-atom MD studies of membrane charge transport have typically been restricted to well-characterized single-component model lipid bilayers (e.g. 16 carbon, dipalmitoyl-PC, DPPC [27]). However, biological membranes can contain a variety of lipid types [28–31], with composition varying widely from membrane to membrane [28,32–33], or even between domains in the same membrane [34–39]. Lipid composition can determine the membrane's shape and mechano-elastic properties [28,33,40], which may influence protein partitioning [41–43] and activity [44–49]. Of all the possible changes in membrane properties, we had anticipated that electrostatic interactions may play an important role in charge–membrane interactions; e.g. via neutralization by binding to a charged lipid [50]. However, we recently demonstrated a surprisingly small effect of anionic lipids on the movement of Arg side chains in membranes, owing to the deformations of the membrane that lead to very similar interactions with zwitterionic and anionic lipids [26]. While there remain a greater variety of lipid chemistries to explore, the next likely suspect for modulating charge–membrane interactions is membrane topology, and in particular its thickness [51–52].

Membranes of differing composition can have considerably different thicknesses, owing to the presence of lipids of different chain length [53], unsaturation [54–56], branching [57], cholesterol [30,58–59] (e.g. cholesterol-rich rafts may be as much as 9 Å thicker than other domains [38]), protein [48,60–65] or cell-perturbing peptides [12,66–67], or due to natural fluctuations in thickness [68]. Membrane hydrophobic thickness is an important factor that affects the structures and activities of many membrane proteins and peptides, such as Na^+,K^+-ATPase [69], rhodopsin [70], mechanosensitive channels [71], potassium channels [72], gramicidin A [73], antimicrobial [66,74] and cell penetrating peptides [12,75]. Notably, the permeabilities of charged and neutral solutes through lipid bilayers are known to be affected by bilayer thickness [51–52]. Here we aim to elucidate the underlying mechanisms and thermodynamics of composition-driven regulation of charge–membrane interactions.

We explore the role of membrane thickness governed by acyl chain length in saturated PC lipid bilayers. Using all-atom MD simulations we will demonstrate an ion-induced defect mechanism where the strains on the bilayer due to membrane deformations result in free energies that grow almost in proportion to thickness, distinct from traditional continuum models that are almost invariant to thickness. We will address recent experiments by calculating the thermodynamics of incorporation of charged protein groups in thick and thin membranes, determine the role of chain length in the Arg protonation state, and investigate the mechanism by which charged groups may move within bilayers, with consequences for the activities of a wide range of membrane proteins and peptides.

2. Computational methods

2.1. Systems

The charged Arg side chain analog, methyl guanidinium ($MguanH^+$), has been used, as in previous studies [25–26,76–78]. Five different PC lipids with saturated hydrocarbon tails of different length have been tested: 18C—DSPC, 16C—DPPC, 14C—dimyristoyl–PC (DMPC), 12C—DLPC, and 10C—didecanoyl-PC (DDPC). The decrease in the number of carbon atoms in the lipid tails leads to systematically reduced membrane thickness (Figs.1 and 2b and c described below, as well as Table S1). We have also simulated the neutral Arg analog, methyl guanidine ($Mguan^0$) in DPPC and DLPC membranes for comparison of pK_a shift calculations (see Fig. 8, to be discussed below). Each system consists of an analog molecule, a 48-lipid bilayer hydrated by a 0.5 M KCl solution (corresponding to 2186 or 2187 water molecules, 20 K^+ and 21 or 20 Cl^- ions for the charged or neutral analog molecule, respectively, to maintain system electroneutrality and sample ionic baths).

Systems were built as in our previous studies, using similar MD simulation protocols [25,77]. For each system, up to 61 umbrella sampling [79] 'window' simulations, for different z positions of the analog molecule across the membrane spanning $-30 \le z \le 30$ Å ($-27 \le z \le 27$ Å and $-25 \le z \le 25$ Å for thinner DLPC and DDPC bilayers, respectively), in 1 Å increments, were performed for ~10 ns each, of which the initial 2 ns was treated as equilibration. The analog center of mass (COM) was held near each umbrella window position by a 2.5 kcal/mol/Å^2 harmonic restraint with respect to membrane COM. The $MguanH^+$ COM lateral distance from the z axis and the lipid bilayer COM along the z axis were constrained using cylindrical and planar constraints of 5 kcal/mol/Å^2 to prevent drifting and thus assist simulation analysis without affecting free energy profiles.

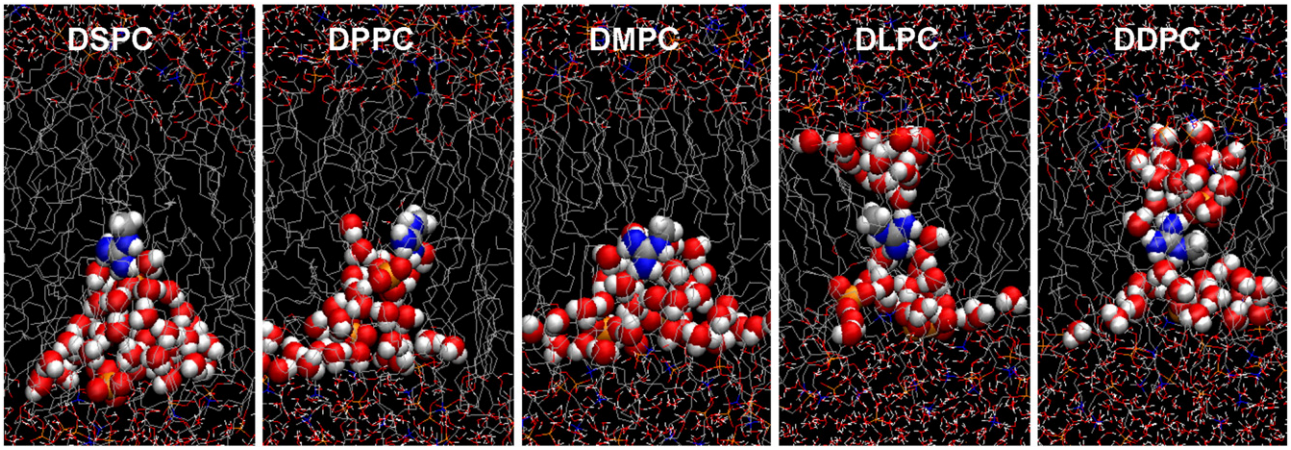

Fig. 1. Equilibrated MD systems for $MguanH^+$ at the center of DSPC, DPPC, DMPC, DLPC and DDPC lipid bilayers; C atoms are shown in gray, H as white, N as blue, O as red, P as orange. $MguanH^+$, together with lipid phosphate and water pulled into the bilayer core, are drawn as balls.

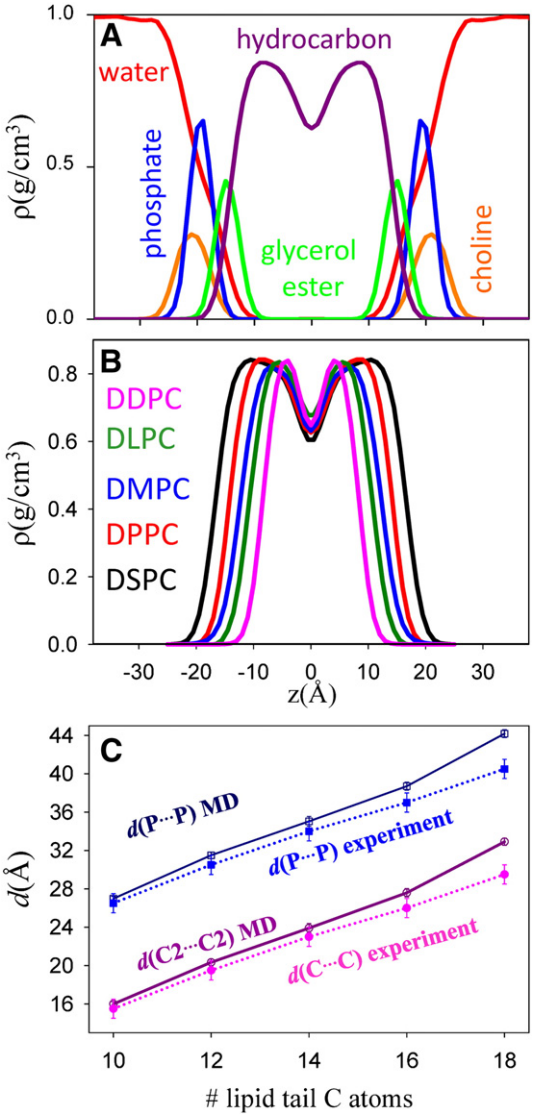

Fig. 2. A) Density profiles for components of an unperturbed DPPC bilayer; B) density profiles of hydrocarbon tail atoms for DSPC (black), DPPC (red), DMPC (blue), DLPC (dark-green) and DDPC (magenta) bilayers; C) bilayer thickness as a function of chain length from MD simulations (solid lines), compared to experiments [53] (dotted lines). Density profiles in panels A and B have been symmetrized with respect to the bilayer center.

2.2. Simulation details

Long-range electrostatics was calculated using the particle-mesh Ewald (PME) method [80], and bonds to H atoms were maintained with the SHAKE algorithm [81]. A real-space non-bond cutoff of 12 Å was used with Lennard–Jones (LJ) interactions truncated via an atom-based force switch algorithm starting at 8 Å. Hexagonal periodic boundary conditions (PBC) were employed along with a Langevin piston [82] and Nose–Hoover [83–84] methods used for coupling pressure and temperature to 1 atm and 318 or 330 K, respectively. Here we employ the newly developed CHARMM C36 force field [85] instead of the C27 [86] and C27r [87] models used previously. The C36 lipid force field reproduces the experimental surface area per lipid and experimental deuterium order parameters in the glycerol and upper chain regions [85]. All simulations have been run in the *NPT* ensemble allowing for independent changes in lateral area and box height, instead of the fixed area, NP_zAT ensemble used in previous studies. Simulations were carried out at 318 K for all 10–16 carbon bilayers, above their gel-phase transition temperatures (up to 314.7 K for DPPC [88]). However, we raised the temperature to 330 K for DSPC, above its transition temperature of 327.5 K [88], but still low enough to be comparable to the other bilayers.

2.3. Simulation analysis

Electron density profiles for different membrane components were obtained by averaging MD frames from unperturbed bilayers. Surface areas per lipid were calculated by averaging the time series of simulation box's dimensions. The head-to-head spacing, d(P···P), was obtained for unperturbed bilayers from the average distance between lipid P atoms in two leaflets, with bilayer core thickness, d(C···C), estimated from C atoms of ester groups, C1, or the 1st carbon of the lipid tails, C2.

Membrane deformations have been gauged by calculating the number of polar membrane components drawn into the bilayer core ($|z| \leq d$(C···C)/2), after shifting the bilayer COM to zero for each frame, where d(C···C) is the experimental hydrocarbon membrane thickness [53], and reported relative to mean numbers for unperturbed bilayers. Values have been plotted either as a function of $MGuanH^+$ position relative to the bilayer center, or as a function of depth inside the hydrocarbon core, based on experimental d(C···C) values from ref. [53]. Experimental d(C···C) values were used for consistency between all-atom MD and continuum membrane calculation results.

Solvation numbers for water, lipid glycerol ester and phosphate oxygen atoms around the guanidine carbon of $MguanH^+$ were obtained by integration of the respective unnormalized radial distribution functions (RDF) out to their first minima. The numbers of hydrogen bonds (H-bonds) between $MguanH^+$ and water, lipid phosphate and glycerol ester groups were calculated with a distance cutoff of 2.5 Å and 120° for the corresponding minimum angle. Interaction energies were computed every 1 ps using a large cutoff of 20 Å, previously shown to yield similar results to PME [77].

PMFs were calculated using umbrella sampling combined with the weighted histogram analysis method [89]. Free energy contributions were obtained by integrating the negative of the mean z-component of the force acting on $MguanH^+$ from particular system components, obtained from calculations every 1 ps using the same nonbonded interaction scheme as used in the MD simulations. For this analysis, "headgroups" refers to the remainder of the lipid molecule without its hydrocarbon tails (from C3 to the terminal C atom); i.e. the combination of both the glycerol ester and phosphocholine moieties. Error bars for all analyses were calculated from asymmetries across the membrane.

2.4. Electrostatic potential calculations from all-atom MD

Electrostatic potentials, φ, were obtained by solution to Poisson's equation using trajectories from MD simulations saved every 100th MD frame (0.2 ps apart), as described previously [25,90]. φ for the unperturbed bilayers were calculated by double integration of averaged electron density along z axis [90]. The PMEPOT plug-in [91] of VMD [92] was used to obtain 2D and 1D profiles using smearing factor $\kappa = 0.34\ Å^{-1}$. The $MguanH^+$ contribution was present in all potential profiles but was negligible for 1D φ profiles across unperturbed bilayers (due to averaging across all x and y values).

2.5. Continuum membrane calculations

Continuum electrostatics was calculated using the PBEQ module of CHARMM. We employ a rigid low-dielectric slab membrane to model a solubility-diffusion process, which excludes the possibility of membrane deformations (although such extensions are possible [93–94]). Membranes were created based on experimental thicknesses, d(C···C) [53]. $MGuanH^+$ was placed at various z positions across the slab

($-25 \le z \le 25$ Å in 0.5 Å increments), and Poisson's equation was solved on a 50x50x100 Å grid with 0.5 Å spacing. The membranes were assigned a dielectric constant 2, surrounded by a solvent with aqueous dielectric constant 80, using a water-sized reentrant probe. Born radii were taken from Refs. [95–96] and partial atomic charges from the C22 force field [97]. The non-polar energy was estimated by multiplying the water-accessible surface of $MGuanH^+$ by a surface tension of 0.033 kcal/mol/Å^2 obtained from alkane–water transfer free energies [98], using boundaries at $|z| = d(C\cdots C)/2$, switched over a 5 Å with a half-Gaussian [99]. A dipole potential contribution was added by scaling C36 results (Fig. S6) down to the experimental value of ~350 mV (e.g. [90,100–101]. See Fig. S5 for different energy components.

3. Results and discussion

3.1. Membrane molecular and charge distributions

The surface areas per lipid of the bilayers (listed in Table S1) reveal very similar values for DPPC, DMPC and DLPC, but an increase by ~3 Å^2 for DDPC, and a decrease by ~3 Å^2 for DSPC. The decrease in area is likely associated with ordering of lipid tails for longer-chain lipids and the fact that the difference between the simulated and gel-phase transition temperature becomes narrower for longer chains. Experimentally very similar areas have been observed for these lipids, regardless of their length [53] in general agreement with these MD simulations, given the uncertainty in the measurements. However, the simulated area for DSPC is ~5 Å^2 too low, likely due to the lower relative temperature used in simulations (just 3 K above the gel transition). This lower area corresponds to a thickening of the membrane that we will show has a small (but non-negligible) effect on Arg translocation energetics.

The density, ρ, profile of an unperturbed DPPC membrane is illustrated in Fig. 2A. The hydrocarbon density profiles for different membranes are compared in Fig. 2B. These profiles are very similar, except for an offset of ~2 Å between neighboring curves due to the systematic change in chain length. This offset is evident in the hydrophobic thickness values, $d(C\cdots C)$, as well as the head-to-head spacings, $d(P\cdots P)$, revealing a systematic decrease from DSPC to DDPC by about 4 Å per 2 chain C atoms, and is within 1–2 Å of experimental data (see Fig. 2C and Table S1). Experimentally, hydrophobic thickness has been determined by subtracting twice the neutron diffraction estimate of phosphate-hydrocarbon distance of 5.5 Å from $d(P\cdots P)$ values [53], or by using the Gibbs dividing surface for the hydrocarbon region based on X-ray and neutron scattering profiles [102]. The former estimates are in a good agreement with our $d(C2\cdots C2)$ values, whereas either $d(C1\cdots C1)$ or $d(C2\cdots C2)$ seem to correspond to experimental estimates obtained using the latter (see Table S1). The largest deviation from experiment occurs for DSPC, by over 3 Å, due to partial ordering of lipid tails at the chosen temperature.

Another membrane property important for charged molecule translocation is the dipole potential, φ, for each bilayer (see Fig. S6), which is positive inside the membrane relative to an aqueous solution and thus thought to impede the permeation of cations [18,103–105]. All membranes have very similar φ profiles, peaked at 700–800 mV at the bilayer center, but shifted according to bilayer thickness. The φ magnitude for DPPC of 706 ± 10 mV is in agreement with a previous study [85], but is smaller than values obtained using C27 model lipids (911 mV [90]; see Fig. S6), previously used to study Arg translocation [21,25–26,76–77]. It is, however, still substantially larger than that calculated using a polarizable membrane model, 500–600 mV [90], as well as experimental estimates of 350–510 mV based on hydrophobic ion translocation [100] and from cryo-electron microscopy of diphytanoyl-PC [101]. These discrepancies might be thought to influence Arg energetics by a few kcal/mol, yet we have previously shown almost no effect, owing to deformations of the bilayer [25,78].

3.2. Membrane deformations due to the presence of Arg

Equilibrated systems with the Arg analog, $MguanH^+$, held at the center of each bilayer, are shown in Fig. 1. Arg leads to deformations by pulling water and phosphate groups into its hydrocarbon core. Despite the number of molecules pulled into the bilayer core, the change in box size in the x–y plane was less than 1%, validating previous studies that sampled from an NP_zAT ensemble, where the error caused by the fixed surface area has been suggested to be small [78].

While in DSPC, DPPC and DMPC the Arg analog pulls water and lipid head groups in from only one interface, in the thin DLPC and DDPC membranes, $MguanH^+$, when within $1-2$ Å of the bilayer center, was observed to grab both sides of the membrane, forming a transmembrane (TM) hydrophobic pore. These pores are partially wetted, or perhaps more appropriately referred to as water wires, in contact with lipid hydrocarbon tails, distinct from wider, fully-wetted TM pores lined by lipid head groups [106]. These pores are similar to those formed by central water defects in our previous study [25], but occluded by an ion in the middle. Similar pores were observed in recent MD simulations of lipid flip-flop across DLPC, DMPC and DPPC membranes by Sapay et al. [107], when the translocating lipid head group was near the membrane center (and up to ~5 Å away for DLPC). The H-bonding capability of $MguanH^+$ may be very important for the stabilization of these pores, as they have not been observed in DLPC membranes with the Lys side chain analog, methyl ammonium, which has reduced H-bonding capacity (Li and Allen, unpublished results). In DDPC and DLPC bilayers, these TM pores appear within the first few ns for several windows and remain stable for more than 20 ns. They depend on position and not initial configuration e.g. disappearing quickly when the analog was moved away from center by 2 Å in DLPC. Such pores are typically not seen in DMPC, except in one simulation, with $MGuanH^+$ held at the bilayer center, where a pore remained stable for 20 ns (not shown).

To gauge the extent of membrane deformations, we calculated the number of polar water (O atom), lipid phosphate (P atom) and choline (N atom) groups inside the membrane core as a function of $MguanH^+$ position (see Fig. 3). The extent of membrane perturbations increases rapidly as $MguanH^+$ moves deeper into membrane core and reaches a maximum near the membrane center. The penetration of water molecules reaches 23 for DDPC to 32 for DPPC (30 for DSPC), and the number of core localized lipid P and N atoms varies from ~2 to 2.5 and ~1 to 1.6, respectively (Fig. 3B). Based on water core penetration numbers it might look as though DPPC, DSPC and DMPC membranes are deformed more than DLPC and DDPC, yet a better comparison can be obtained by examining the deformations as a function of depth from the edge of the hydrocarbon cores of the membrane, rather than distance from the bilayer centers. When this is done, the core numbers become very similar for all bilayers (inset of Fig. 3A), despite pore formation in DLPC and DDPC bilayers.

3.3. Solvation, H-bonds and interaction strengths

The solvation numbers characterizing the micro-environment of $MguanH^+$ at each position across the membrane are shown in Fig. 4A for DLPC and DPPC membranes (with results for all lipids used in this study presented in Fig. S2). In bulk aqueous solution, $MguanH^+$ is surrounded by ~12 water molecules in its 1st solvation shell (a high number based on the distribution around the guanidine C atom, and not H-bonding to the amine groups). This number decreases to 4–6 in the interfacial regions and stays nearly constant throughout the membrane. In the interfacial region the charged analog is coordinated by 3–4 phosphate and 2–3 glycerol ester O atoms. Near the membrane center $MguanH^+$ is coordinated by ~5 water molecules, 1–2 phosphate oxygen atom and ~1 glycerol ester oxygen in DPPC and DLPC bilayers (Fig. 4A), with similar numbers for other lipids (see Fig. S2). The total solvation number (black curves in Fig. 4A) gradually decreases from ~12 in bulk aqueous solution to 6–8 near the membrane center,

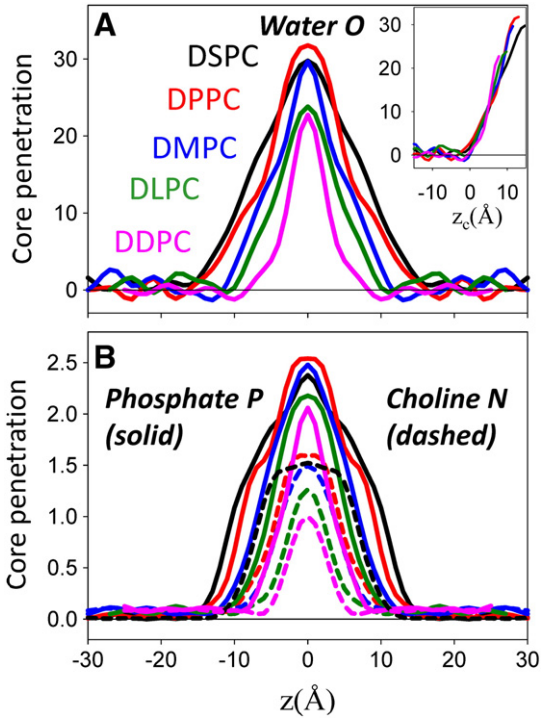

Fig. 3. Number of polar species inside the membrane core (with respect to unperturbed bilayers). A) water O atoms, B) lipid phosphate P (solid lines) and choline N (dashed lines) as a function of MguanH$^+$ position across the membrane. The membrane core has thickness 29.5 Å (DSPC), 26 Å (DPPC), 23 Å (DMPC), 19.5 Å (DLPC), or 15.5 Å (DDPC) from Ref. [53]. Core penetration profiles have been symmetrized with respect to MguanH$^+$ position at the bilayer center ($z=0$). The inset in panel A shows the number of water O atoms in the membrane core as a function of MguanH$^+$ distance from the interface/core boundary, z_c.

with the difference between DPPC and DLPC profiles being an expected offset due to the differing bilayer thicknesses. TM pores in DDPC and DLPC do not significantly affect solvation numbers, which are similar to DMPC, DPPC and DSPC results (Fig. S2; with deviations for DLPC and DDPC being comparable to the error bars). The comparison of C36 with previous C27 results for DPPC [77] (see Fig. S1A) shows very similar solvation numbers (with a slight decrease in interfacial phosphate and increase in glycerol ester binding in C36).

H-bond numbers are also very similar between different bilayers, again with an expected shift of ~2 Å between successive chain lengths (see. Fig. 4B and Fig. S3). The total number of H-bonds (black curves) is ~4.5 in bulk water, reaching ~5 in the membrane and staying nearly constant across the membranes. There are, however, large variations in the contributions from individual membrane components. In bulk aqueous solution and near the membrane center, contributions from water are dominant. In the interfacial and outer core regions, the water contribution decreases to ~1–2 and more than half of the H-bonds to MguanH$^+$ are formed by lipid phosphates (~2–3) and glycerol ester (~0.5–1.5 groups). In comparison to our previous C27 results [77], phosphate groups form fewer H-bonds with MguanH$^+$, while glycerol ester groups form more, leading to an unchanged total number of H-bonds (see Fig. S1B). This may be explained by the larger glycerol ester dipole in C36 [85].

Interaction energies of MguanH$^+$ with lipid head groups, water and ions, as well as the total interaction energy, are plotted in Fig. 4C for DLPC and DPPC (see Fig. S4 for all lipids). The interactions of MguanH$^+$ with all lipids are similar, allowing for the expected shifts. MguanH$^+$ interacts with lipid head groups and water molecules strongly throughout the membrane, which can account for the observed deformations [21,77]. Interactions with water molecules are largest in the bulk aqueous solution (~−100 kcal/mol), weakening to nearly 0 in the interfacial region, but strengthening again to ~−50 kcal/mol near the membrane

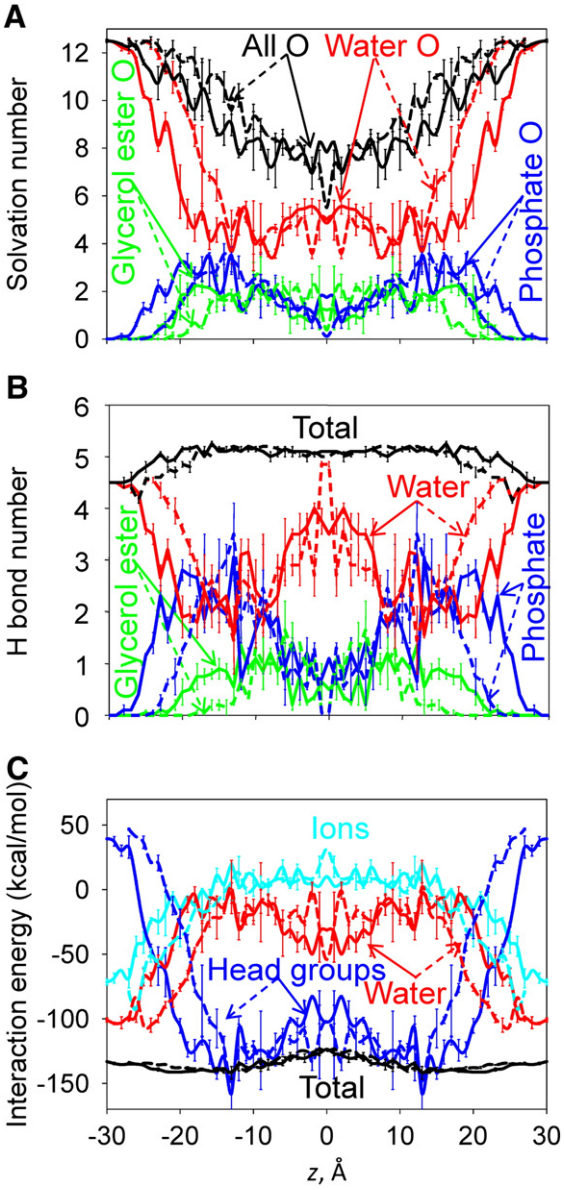

Fig. 4. MguanH$^+$ interactions with DPPC (solid lines) and DLPC (dashed lines) membranes: A) Mean first-shell solvation numbers for water O (red), phosphate O (blue), and glycerol ester O atoms (green), defined by minima in the RDFs of radii 4.85, 4.55, and 5.00 Å, respectively, relative to guanidine carbon as in ref. [21]. B) The H-bond numbers by water, phosphate, and glycerol ester. An H-bond D-H···A is counted when the distance H···A < 2.5 Å, and angle D-H···A > 120°. C) Average side chain interaction energies for MguanH$^+$ with components: water (red), lipid head groups, including glycerol ester moieties (blue), K^+ and Cl^- ions (cyan). Sums of these components are shown by black lines in each panel. All profiles have been symmetrized with respect to the MguanH$^+$ position at the bilayer center ($z=0$), and the error bars represent a measure of asymmetry. See Figs. S2, S3 and S4 for all lipid membranes used in this study.

center. Interactions with lipid head groups reach ~−150 kcal/mol in the interfacial regions, and remain strong (~−100 kcal/mol) to drive these polar groups into the hydrophobic core. Interactions with salt ions in aqueous solution are also quite strong, (up to ~−70 kcal/mol) yet vanish inside the bilayer, indicating a strong preference for binding to lipid phosphates over counter-ions there. Interaction energy profiles for C36 and C27 force fields are very similar (Fig. S1C).

3.4. Free energy profiles

The PMFs governing membrane translocation of MguanH$^+$ through the different bilayers (Fig. 5A) are very similar in shape, shifted by ~2 Å

between successive chain lengths. Similar slopes indicate comparable forces expelling MguanH$^+$ from the bilayer cores, consistent with the similar deformations observed above. Each PMF has a distinctive Λ shape since the ion never crosses the membrane interface, but deforms it, moving against an almost constant opposing force [25].

The PMFs for different chain lengths have similar weak interfacial binding, but different barrier heights, simply because the force acting to expel the ion is similar, but integrated over a different thickness. The inset in Fig. 5A reveals just how similar the PMFs are when plotted as a function of depth in from the interface instead of distance from the bilayer center. Because the mean force acting on the charged analog is ~1.5 kcal/mol/Å on average (1.2–1.8 kcal/mol/Å, increasing with chain length), the change in thickness can capture much of the drop in barrier height with decreasing chain length. However, MguanH$^+$ causes TM pores to form in DLPC or DDPC bilayers, eliminating net force toward either interface and leading to plateaus in their PMFs (Fig. 5A), similar to lipid flip-flop PMFs from a previous study [107]. One may anticipate a further decrease in barrier due to this pore formation. However, while pore formation in the thin bilayers does halt the rapid climb in free energy with ion movement, the work has already been done for the ion to reach that point. We also note that the PMFs from C36 (here) and C27 [77] are the same to within ~0.5 kcal/mol.

To help understand the origin of any differences in these PMFs for different chain lengths, we have broken them down into contributions from different membrane components via a mean force decomposition (Fig. 6). Contributions from water, lipids and ions are presented (with the latter two combined). As with the total PMF, the forces coming from individual components as the ion enters the membrane are similar for all bilayers, but the curves are shifted because of the differing thicknesses. It is only deep inside the interfaces that differences become apparent. In the interfacial region, dehydration (water; solid lines) leads to strongly unfavorable contributions, cancelled by opposing lipid + ion contributions (dashed lines). In the middle of the bilayers, water becomes more stabilizing while lipids + ions are more destabilizing, with the net result leading to barriers in the PMFs (dotted lines).

We can understand a trade-off between water and lipids by considering the competition for binding in each region of the bilayer. As MGuanH$^+$ moves from bulk water into the interface, the mole fraction of water is reduced (and MGuanH$^+$ must compete with head groups for hydration), leading to a repulsive free energy contribution (a more detailed discussion, including enthalpic and entropic contributions to this repulsion, can be found in Ref. [77]). In contrast, the free energy contribution from lipid head groups is attractive as the ion moves from water into the interface (Fig. 6). As the ion moves deeper into the membrane, water molecules are drawn into the core and are very effective at stabilizing charges away from the aqueous phase [108], leading to forces that push the ion from the interface into the core. However, when lipid head groups are displaced to coordinate the ion in the core, the associated energetics will lead to forces directing the ion back toward the interface. While these counteracting forces are roughly in balance at the interface, their net effect inside the core is strongly repulsive.

In the thicker membranes, the deeper the ion moves into the core, the more strained the displaced head groups become, leading to an ever growing repulsive PMF contribution that eventually dominates. In DSPC, DPPC and even DMPC, the lipid contribution keeps climbing all the way to the bilayer center (in all three cases being positive in free energy at the center), while the water contribution keeps falling all the way to the center (in all three cases being negative in free energy at the center). However, a noticeable difference can be seen for DLPC and DDPC, where the bilayers are too thin for the head group contribution to become positive (and for the water contribution to become attractive). As a result, we would argue that with the ion near the center of DLPC or DDPC bilayers, lipid head groups come and go with greater ease than in the thicker membranes, with the inevitable outcome of pore formation.

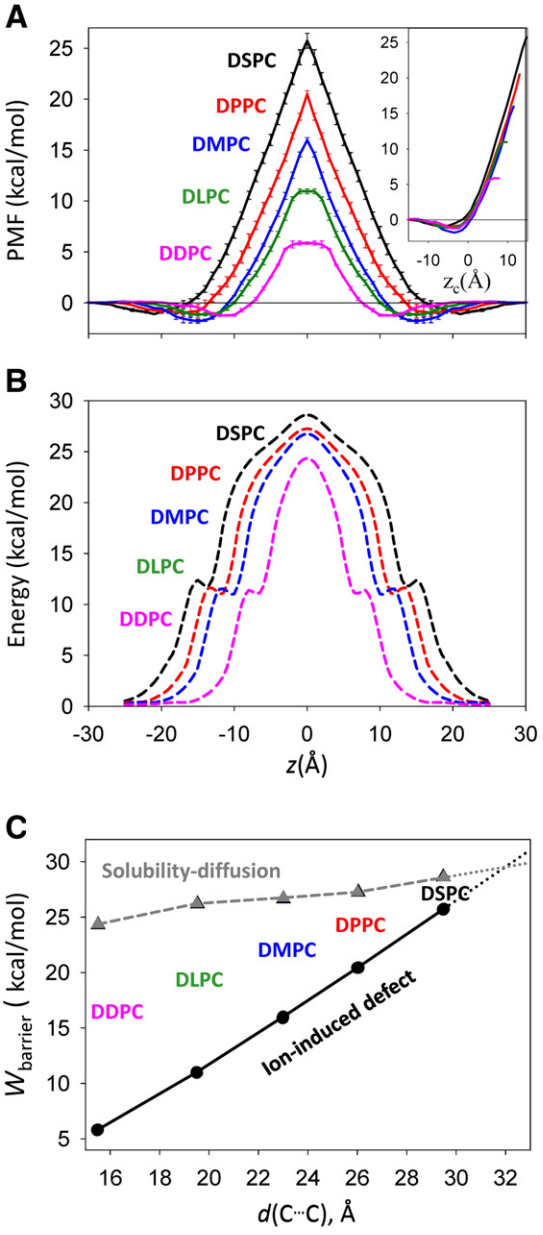

Fig. 5. A) PMFs of MguanH$^+$ translocation across DSPC (black), DPPC (red), DMPC (blue), DLPC (dark-green) and DDPC (magenta) membranes from all-atom simulations. The inset shows PMFs as a function of MguanH$^+$ distance from the interface/core boundary, z_c. Error bars have been computed as in Fig. 4. B) Energies of MguanH$^+$ across membranes of different thickness from continuum membrane calculations (see Fig. S5 for individual energy components). C) Free energy barriers for MguanH$^+$ as a function of bilayer thickness (all-atom MD—solid black, continuum—dashed gray curve). Linear extrapolations are drawn with dotted lines.

The overall barrier heights, $W_{barrier}$, increase linearly with hydrophobic membrane thickness, d(C···C), from 5.8 kcal/mol for DDPC to 25.7 kcal/mol for DSPC (a slope of 1.4 kcal/mol/Å of thickness; Fig. 5C). Thus, while previously the cost of unassisted translocation of Arg has been deemed prohibitively high [21], we now see that in thin membranes the cost can be quite low. We have to also remember that this is the cost of moving a lone side chain analog molecule into the bilayer. In contrast, experiments have relied on measurements involving the partitioning of host peptides [109] or entire β barrel proteins [3], where the Arg side chain would snorkel and the protein segment itself would be expected to drift due to the forces acting on the Arg. We have previously shown that snorkeling reduces the free energy of an Arg placed in the middle of a bilayer by up to 3 kcal/mol [77]. We have

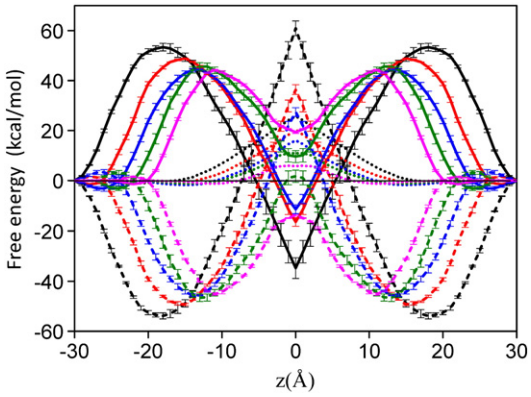

Fig. 6. Free energy contributions for $MguanH^+$ translocation across DSPC (black), DPPC (red), DMPC (blue), DLPC (dark-green) and DDPC (magenta) bilayers from force decomposition analysis. Water (solid lines), lipid and ion (dashed lines) and total PMFs (dotted lines) are shown (error bars computed as in Fig. 4).

also shown that a single hydrophobic helix flanked by prolines and charged residues may slide by 8–10 Å [21], consistent with experiments [110], while a WALP peptide may slide by up to 5 Å if an Arg is placed at the center (Chen and Allen, unpublished results), and undergo significant tilts that can bring the guanidinium group closer to the interface [111]. Significantly, even small displacements (just a couple of Å) of the host protein lead to significant stabilization of Arg, owing to the steep slope of the Arg side chain PMF (~1.5 kcal/mol/Å). One may therefore expect free energy penalties for incorporating Arg into a TM segment to be just a few kcal/mol in DDPC or DLPC membranes, consistent with recent experiments [3]. We remark, however, that a quantitative comparison is difficult, given the different systems, especially due to the presence of a partially water-filled OmpLA pore that will help stabilize charges inside the membrane, as well as consideration of the appropriate reference states (Ref. [3] reports free energies relative to alanine, and also relative to an unfolded state of unknown free energy).

3.5. Ion-induced defect versus solubility diffusion

While the implications of the low barriers for Arg movement into thin bilayers maybe significant, the growing barriers in thick membranes have their own consequences. Based on bulk solvent partitioning, employing a Born energy description, the cost of Arg movement from water ($\varepsilon = 80$) to hydrocarbon ($\varepsilon = 2$) is ~31 kcal/mol (i.e. negative one half of its hydration free energy of ~−62 kcal/mol [78]). The barrier for Arg translocation across DSPC from all-atom MD simulations is approaching this limiting value, suggesting a possible transition from an ion-induced defect to a solubility-diffusion mechanism [112], entailing complete or partial [51–52] dehydration without significant membrane deformations. We now seek a more quantitative analysis of this competition between mechanisms.

Continuum membrane models have been traditionally used to estimate the energetics for ion translocation across rigid low-dielectric slab membranes [18,113], despite the limitations that by now are clearly evident. We have calculated the cost of moving $MguanH^+$ into the membrane via solution to Poisson equation (dominated by the dehydration penalty, as well as a smaller interaction with the dielectric boundary [19]), a non-polar contribution arising from the costs of cavity formation in water and hydrocarbon (~−9 kcal/mol for all lipids, somewhat overestimated compared to atomistic simulations [90]), and due to the dipole potential (8–9 kcal/mol for all lipids). Given the approximate cancellation of non-polar and dipole potential terms, the energetics (shown in Fig. 5B) are governed almost exclusively by dehydration (with a decomposition provided in Fig. S5). All energy profiles lack the characteristic Λ shape of the all-atom PMFs (compare Fig. 5B and A). Significantly, the barriers calculated do not yield the same dependence on bilayer thickness (Fig. 5C, dashed curve) as seen in all-atom simulations (solid curve). While the energy barriers exhibit shifts due thickness changes, the continuum model incorrectly captures only a dehydration effect that is common to all bilayers. As a result, the barrier only drops from 28.6 kcal/mol for DSPC to 24.3 kcal/mol for DDPC.

According to the all-atom simulations, we would predict dramatic reductions in translocation rates across membranes with increasing membrane thickness (a thorough study of ion diffusion and permeation rates with comparison to experiments to be submitted). The increase in barrier height should correspond to about 3 orders of magnitude increase in permeability per 2 carbon atoms in the lipid tails. In contrast, the continuum membrane model predicts very little sensitivity to membrane thickness. Previous experiments in a range of mono-unsaturated lipids have observed little sensitivity of K^+ ion permeability to chain lengths of 18−24 carbons, corresponding to membrane hydrophobic thicknesses of 27.0−37.5 Å [51], mostly above the range explored here. This experimental evidence suggests that in thick membranes, a solubility-diffusion mechanism is dominant. However, deviations were observed in bilayers thinner than ~27 Å (corresponding roughly to DPPC), suggested to be associated with the onset of a transient pore mechanism [51]. In our study, the barriers to ion-induced defect formation become lower than solubility-diffusion (dehydration) in thin membranes; though we cannot exclude the contribution from transient pores. We recognize that lipid unsaturation, with corresponding changes in membrane properties [107], will affect the switch between ion-induced pore formation and the solubility-diffusion mechanism, while the difference in $MGuanH^+$ and K^+ hydration energetics, of ~20 kcal/mol, is expected to have an even greater influence on this transition. Moreover, our model to predict the transition between ion-induced defect-facilitated and solubility-diffusion assumes complete dehydration of the ion, for the latter mechanism, which may not be the case. Due to these factors we hesitate to provide direct quantitative comparisons with experiments performed on different model systems [51]. What is indisputable, however, is that the two curves in Fig. 5C must intersect at some point, possibly in the vicinity of 18–20C atoms, indicating a switch between different translocation mechanisms.

While we did not see the breaking of interfacial connections leading to solubility-diffusion translocation of $MGuanH^+$, even in DSPC bilayers, such a transition has been observed recently for the case of lipid flip-flop in membranes thickened by cholesterol [114]. This may be due to the non-polarizable all-atom simulations suffering from an inadequacy that may prohibit such changes. As shown above (Fig. 5C), the cost of ion-induced translocation in thick membranes has reached a level comparable to that for dehydrating the ion. However, in a non-polarizable MD simulation, the energetic cost of solubility-diffusion [78,90] is overestimated by a factor of up to 2 because the dielectric constant of the hydrocarbon core is around 1 instead of 2 [115]. Thus, solubility-diffusion in a non-polarizable MD simulation might never occur, unless the membrane is very thick, or the ion remains partly hydrated [51]. This highlights the need for explicit treatment of electronic polarizability for a quantitative exploration of the mechanisms of translocation in thick membranes.

3.6. Electrostatics of deformable membranes of different thickness

The dipole potential is one of the key factors governing ion translocation in the traditional solubility-diffusion model [104]. This potential is large (~350–510 mV), corresponding to an additional penalty of up to 12 kcal/mol for $MGuanH^+$ to cross a membrane. For the C36 and C27 MD models, this term is higher (by at least ~200 and 400 mV, respectively; Fig. S6), corresponding to changes in the energy of a bare ion by 4.5–9 kcal/mol. Despite model variations in dipole potential, the PMFs for $MGuanH^+$ across C36 and C27 membranes differ by just ~0.5 kcal/mol. Moreover, similar changes in the dipole potential, due to the incorporation of electronic polarizability of the lipid chains,

had almost no effect on the resultant PMFs since the ion does not feel the full dipole potential due to membrane deformations [25].

The 2D electrostatic potential maps for the unperturbed membranes clearly reveal the change in bilayer thickness, affecting the spread but not the magnitude of the potential (top panels of Fig. 7). As a result of $MGuanH^+$ perturbing the bilayer, the low-potential region of the bulk solution extends to just a few Å from the membrane center (bottom panels of Fig. 7; with more bilayers shown in Fig. S7 and 1D projections in Fig. S8). The ion itself is located near the interface between low- and high-potential regions, and never completely crosses between them [25]. In the case of the thin DLPC membrane (as well as DDPC; Fig. S7), we see that the membrane deformations and corresponding low-potential regions extend to both leaflets, with $MGuanH^+$ residing in the middle. For DSPC, DPPC and DMPC membranes, $MGuanH^+$ is located at a high-electric field position (riding a steep slope in potential; Fig. S8), thus experiencing a large force expelling it from the membrane and accounting for the Λ shape of the PMF [25]. For DDPC and DLPC membranes, $MGuanH^+$ is located in a high-potential region, but resides at the top of the barrier with zero slope, and thus experiences zero electric field expelling it from the membrane (see Fig. 7 and S8), corresponding to the plateaus in the PMFs.

We remark that, irrespective of the bilayer thickness, it is the leading charge (i.e. $MGuanH^+$) that is feeling the force expelling it from the membrane, with the coordinating phosphate in a region of reduced potential and field, and the choline essentially feeling no force at all [25]. We have previously suggested that this can explain why an anionic lipid (possessing the phosphate but no cationic moiety) has very little effect on the PMF for Arg translocation [26], and have used this leading charge hypothesis to predict a common energetics for a range of ions, zwitterions and polyionic biomolecules [25–26], as has been shown computationally [116], and experimentally [3] for Arg pairs.

3.7. pK_a shift of Arg in bilayers of different thickness

We now discuss the consequences of the varying free energy costs for charged Arg movement into bilayers of different thickness on its protonation state. Despite the high aqueous pK_a of 13.4 (for $MGuanH^+$[117]), neutralization, if it were to occur, would lower the translocation barrier. Continuum theory predicts that the cost of translocation of the charged species is so high that deprotonation is certain inside a membrane [78], yet we know that those energetics have been exaggerated by the rigid dielectric model. We have previously shown, using all-atom MD simulations, that $MGuanH^+$ would undergo pK_a shifts that grow steeply as the molecule moves deeper into the membrane, with the pK_a eventually dropping below 7 at the center of a DPPC bilayer (also shown in Fig. 8C) [76–77]. However if the Arg side chain is attached to a host protein and allowed to snorkel, Arg would actually remain protonated, even at the bilayer center (at neutral pH) [76–77]. The reason for these low shifts is the reduction in barrier for the protonated form due to membrane deformations, and the fairly high costs of dehydrating the neutral side chain [76–77]. However, thinning of the membrane will further reduce these shifts, which we now explore.

We have computed the PMFs for the neutral Arg analog, $Mguan^0$, moving across DPPC and DLPC bilayers (Fig. 8B). The free energy barriers for $Mguan^0$ are determined by simple dehydration (maintaining on average, just ~0.6 waters in DLPC and ~0.2 in DPPC), leading to different shapes to those for the charged analog. In DPPC, the barrier becomes flat once dehydration is complete, while DLPC is only just thick enough to lead to a similar level of dehydration, so that a plateau is not seen (though the barrier heights are almost the same; 8.6 Vs 8.5 kcal/mol). If not for the shift due to bilayer thickness, the PMFs in DLPC and DPPC would be essentially identical (not shown). We note that the C36 barrier for $Mguan^0$ in DPPC is similar, but 1.5 kcal/mol higher than our previous C27 result [77].

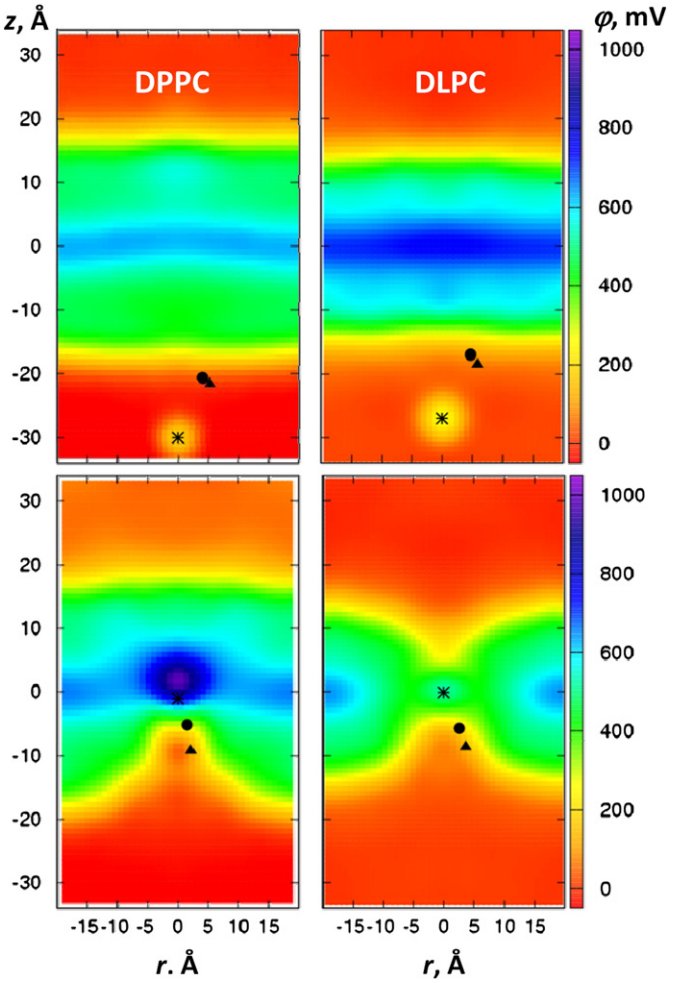

Fig. 7. 2D electrostatic potential maps along the z axis and distance r from the z axis when the $MguanH^+$ ion is in aqueous solution (top) and near the membrane center ($z \approx 0$ Å, bottom) for DPPC (left) and DLPC (right) membranes. 2D maps for all lipid bilayers and corresponding 1D projections are shown in Figs. S7 and S8, respectively. All maps have been symmetrized with respect to $r = 0$. The average positions of the guanidine C and its closest lipid P and N atoms are shown as black asterisk, circle, and triangle, respectively. The corresponding system snapshots for the deformed bilayers in the bottom row are shown in Fig. 1.

The cost of $MguanH^+$ deprotonation across the membrane, $\Delta\Delta G_{deprot}(z)$, can be calculated as $W_{Mguan^0}(z) - W_{MguanH^+}(z)$ (explained in Refs. [76–77], via a thermodynamic cycle) and the corresponding $\Delta pK_a(z)$ profiles obtained as $\Delta\Delta G_{deprot}(z)/(2.303\ k_BT)$. The $\Delta pK_a(z)$ profiles across DLPC and DPPC membranes (Fig. 8C) indicate a small positive pK_a shift up to 2 units in the interfacial region due to $MGuanH^+$ binding, which then drops inside the membrane core due to destabilization of the charged species. For DPPC, the pK_a drops by up to 8.1 units (falling from over 13 to below 6; red curve), whereas for DLPC the shift never exceeds −1.9 units (dark-green curve). This proves that Arg, even as a lone side chain analog molecule, would always remain protonated in thin membranes (the pK_a never dropping below around 11 units), but that in thick membranes (DPPC or greater), deprotonation at the membrane center would occur (noting again that the ability to snorkel on a host protein will reduce these shifts [77]).

4. Conclusions

We have carried out atomistic simulations of the translocation of the Arg side chain analog, $MguanH^+$, across lipid membranes with systematically changed hydrophobic thickness. We discovered that $MguanH^+$ leads to similar membrane deformations in all bilayers by pulling water

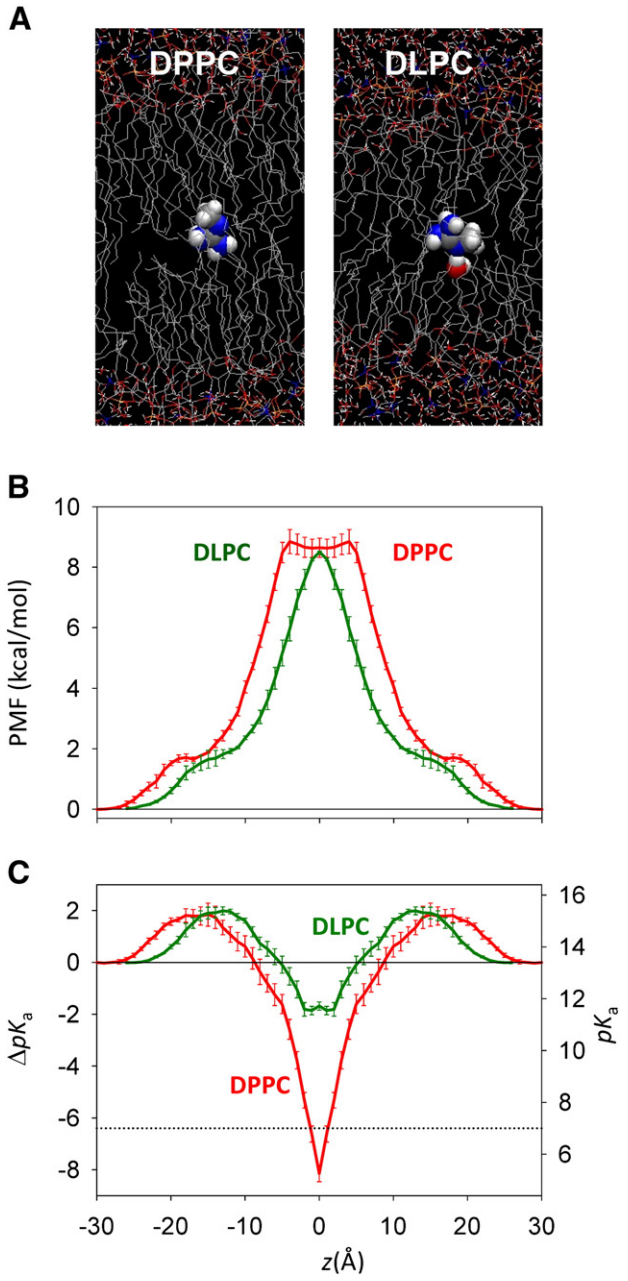

Fig. 8. A) Equilibrated MD systems for $Mguan^0$ at the center of DPPC and DLPC bilayers. B) PMFs of $Mguan^0$ across DPPC (red) and DLPC (dark-green) membranes. C) pK_a shift profiles for DPPC and DLPC bilayers, based on $MguanH^+$ and $Mguan^0$ PMFs (error bars computed as in Fig. 4).

molecules and lipid head groups into their hydrocarbon cores. The solvation, H-bonding and interaction energies of $MguanH^+$ in these membranes are very similar, except for a shift caused by the change in bilayer hydrophobic thickness. We found that if results are plotted as a function of distance from the interface instead of the bilayer center, the deformations and ion microenvironments are very similar in all bilayers.

All translocation free energy profiles exhibit a shape that is characteristic of an ion-induced defect translocation mechanism, with similar slopes, and a central barrier varying from just 5.8 kcal/mol for DDPC to as high as 25.7 kcal/mol for DSPC, scaling almost linearly with a membrane thickness. In thin membranes, such as DLPC or DDPC, $MguanH^+$ pulls water and head groups from both sides of the membrane to form a hydrophobic TM pore, in which the ion can move freely near the membrane center. Our analysis of contributions to the free energy suggests a situation where DDPC and DLPC are thin enough so that the movement of lipid head groups into the deformed membrane has not yet become too unfavorable, promoting pore formation. The lowering of the barriers in thin membranes, after accounting for further reductions that would occur due to side chain snorkeling and host protein movements, as a result of the large forces on the Arg side chain, are expected to be in accord with recent experiments [3].

The systematic dependence of the translocation barrier on membrane thickness, which is not observed in continuum membrane models, leads to important conclusions in regards to the mechanism by which charged molecules, such as Arg, traverse lipid bilayers. We have predicted that all such translocations would be mediated by ion-induced defect-mediated diffusion (in the absence of transient pores, not investigated here), where the ion remains hydrated at the deformed interface, as opposed to a traditional solubility-diffusion mechanism where the ion partitions from water to hydrocarbon and diffuses the membrane core [51]. Our results indicate, however, that solubility-diffusion would become the preferred translocation mechanism in thicker membranes, at least as thick as DSPC, though with some uncertainty, owing to the absence of explicit membrane electronic polarizability.

We showed that because the barrier height for the charged Arg analog is so sensitive to thickness in the all-atom description, and that of the neutral analog is not, $MGuanH^+$ would experience deprotonation at the centers of thick membranes, but not in thin membranes, whereas the continuum description would incorrectly predict deprotonation throughout all membranes. This important effect of membrane thickness on the protonation state of a titratable protein side chain would not have been captured in traditional implicit membrane models. We have also discussed how the membrane deformations within leaflets of the thick membranes, or as TM pores in thin membranes, control the energetics of translocation and govern a general insensitivity to ion type, ion pairs or polyionic biomolecules, with implications for a range of charged proteins and cell-perturbing peptides in nature.

Acknowledgements

We would like to acknowledge funding from NSF (awards MCB-0546768 and MCB-1052477) and supercomputing support from Teragrid (award MCB-050005).

Appendix A. Supplementary data

Supplementary data to this article can be found online at doi:10.1016/j.bbamem.2011.10.026.

References

[1] Y.X. Jiang, V. Ruta, J.Y. Chen, A. Lee, R. MacKinnon, The principle of gating charge movement in a voltage-dependent K+ channel, Nature 423 (2003) 42–48.
[2] T. Hessa, H. Kim, K. Bihlmaier, C. Lundin, J. Boekel, H. Andersson, I. Nilsson, S.H. White, G. von Heijne, Recognition of transmembrane helices by the endoplasmic reticulum translocon, Nature 433 (2005) 377–381.
[3] C.P. Moon, K.G. Fleming, Side-chain hydrophobicity scale derived from transmembrane protein folding into lipid bilayers, Proc. Natl. Acad. Sci. U. S. A. 108 (2011) 10174–10177.
[4] C.M. Armstrong, F. Bezanilla, Currents related to movement of the gating particles of the sodium channels, Nature 242 (1973) 459–461.
[5] R.A. Mathies, S.W. Lin, J.B. Ames, W.T. Pollard, From femtoseconds to biology—mechanism of bacteriorhodopsins light-driven proton pump, Annu. Rev. Biophys. Biophys. Chem. 20 (1991) 491–518.
[6] M. Rudiger, D. Oesterhelt, Specific arginine and threonine residues control anion binding and transport in the light-driven chloride pump halorhodopsin, EMBO J. 16 (1997) 3813–3821.
[7] A.M. Powl, J. Carney, P. Marius, J.M. East, A.G. Lee, Lipid interactions with bacterial channels: fluorescence studies, Biochem. Soc. Trans. 33 (2005) 905–909.
[8] D. Schmidt, Q.X. Jiang, R. MacKinnon, Phospholipids and the origin of cationic gating charges in voltage sensors, Nature 444 (2006) 775–779.
[9] F.I. Valiyaveetil, Y.F. Zhou, R. Mackinnon, Lipids in the structure, folding, and function of the KcsA K+ channel, Biochemistry USA 41 (2002) 10771–10777.

[10] J. Payandeh, T. Scheuer, N. Zheng, W.A. Catterall, The crystal structure of a voltage-gated sodium channel, Nature 475 (2011) 353–358.
[11] M. Zasloff, Antimicrobial peptides of multicellular organisms, Nature 415 (2002) 389–395.
[12] H.D. Herce, A.E. Garcia, Cell penetrating peptides: how do they do it? J. Biol. Phys. 33 (2007) 345–356.
[13] K. Melikov, L. Chernomordik, Arginine-rich cell penetrating peptides: from endosomal uptake to nuclear delivery, Cell. Mol. Life Sci. 62 (2005) 2739–2749.
[14] K.M. Wagstaff, D.A. Jans, Protein transduction: cell penetrating peptides and their therapeutic applications, Curr. Med. Chem. 13 (2006) 1371–1387.
[15] A.S. Ladokhin, S.H. White, 'Detergent-like' permeabilization of anionic lipid vesicles by melittin, Biochim. Biophys. Acta 1514 (2001) 253–260.
[16] H.J. Jung, J.Y. Lee, S.H. Kim, Y.J. Eu, S.Y. Shin, M. Milescu, K.J. Swartz, J.I. Kim, Solution structure and lipid membrane partitioning of VSTx1, an inhibitor of the KvAP potassium channel, Biochemistry USA 44 (2005) 6015–6023.
[17] M. Milescu, J. Vobecky, S.H. Roh, S.H. Kim, H.J. Jung, J. Il Kim, K.J. Swartz, Tarantula toxins interact with voltage sensors within lipid membranes, J. Gen. Physiol. 130 (2007) 497–511.
[18] B.H. Honig, W.L. Hubbell, R.F. Flewelling, Electrostatic interactions in membranes and proteins, Annu. Rev. Biophys. Biophys. Chem. 15 (1986) 163–193.
[19] A. Parsegian, Energy of an ion crossing a low dielectric membrane: solutions to four relevant electrostatic problems, Nature 221 (1969) 844–846.
[20] M.A. Wilson, A. Pohorille, Mechanism of unassisted ion transport across membrane bilayers, J. Am. Chem. Soc. 118 (1996) 6580–6587.
[21] S. Dorairaj, T.W. Allen, On the thermodynamic stability of a charged arginine side chain in a transmembrane helix, Proc. Natl. Acad. Sci. U. S. A. 104 (2007) 4943–4948.
[22] A.C.V. Johansson, E. Lindahl, The role of lipid composition for insertion and stabilization of amino acids in membranes, J. Chem. Phys. 130 (2009) 185101.
[23] J.L. MacCallum, W.F.D. Bennett, D.P. Tieleman, Partitioning of amino acid side chains into lipid bilayers: results from computer simulations and comparison to experiment, J. Gen. Physiol. 129 (2007) 371–377.
[24] J.A. Freites, D.J. Tobias, G. von Heijne, S.H. White, Interface connections of a transmembrane voltage sensor, Proc. Natl. Acad. Sci. U. S. A. 102 (2005) 15059–15064.
[25] I. Vorobyov, B. Bekker, T.W. Allen, Electrostatics of deformable lipid membranes, Biophys. J. 98 (2010) 2904–2913.
[26] I. Vorobyov, T.W. Allen, On the role of anionic lipids in charged protein interactions with membranes, Biochim. Biophys. Acta 1808 (2011) 1673–1683.
[27] D.P. Tieleman, S.J. Marrink, H.J. Berendsen, A computer perspective of membranes: molecular dynamics studies of lipid bilayer systems, Biochim. Biophys. Acta 1331 (1997) 235–270.
[28] R. Gennis, Biomembranes: Molecular Structure and Function, Springer, New York, 1989.
[29] B. Brugger, G. Erben, R. Sandhoff, F.T. Wieland, W.D. Lehmann, Quantitative analysis of biological membrane lipids at the low picomole level by nano-electrospray ionization tandem mass spectrometry, Proc. Natl. Acad. Sci. U. S. A. 94 (1997) 2339–2344.
[30] H. Sprong, P. van der Sluijs, G. van Meer, How proteins move lipids and lipids move proteins, Nat. Rev. Mol. Cell Biol. 2 (2001) 504–513.
[31] A. Shevchenko, K. Simons, Lipidomics: coming to grips with lipid diversity, Nat. Rev. Mol. Cell Biol. 11 (2010) 593–598.
[32] G. van Meer, D.R. Voelker, G.W. Feigenson, Membrane lipids: where they are and how they behave, Nat. Rev. Mol. Cell Biol. 9 (2008) 112–124.
[33] A.M. Dopico, G.J. Tigyi, A glance at the structural and functional diversity of membrane lipids, in: A.M. Dopico (Ed.), Methods in Membrane Lipids, Humana Press, Totowa, N.J., 2007, pp. 1–13.
[34] K. Simons, E. Ikonen, Functional rafts in cell membranes, Nature 387 (1997) 569–572.
[35] M. Edidin, Lipid microdomains in cell surface membranes, Curr. Opin. Struct. Biol. 7 (1997) 528–532.
[36] D.A. Brown, E. London, Structure and origin of ordered lipid domains in biological membranes, J. Membr. Biol. 164 (1998) 103–114.
[37] K. Jacobson, C. Dietrich, Looking at lipid rafts? Trends Cell Biol. 9 (1999) 87–91.
[38] M. Gandhavadi, D. Allende, A. Vidal, S.A. Simon, T.J. McIntosh, Structure, composition, and peptide binding properties of detergent soluble bilayers and detergent, resistant rafts, Biophys. J. 82 (2002) 1469–1482.
[39] J.C. Holthuis, G. van Meer, K. Huitema, Lipid microdomains, lipid translocation and the organization of intracellular membrane transport (Review), Mol. Membr. Biol. 20 (2003) 231–241.
[40] R.M. Epand, Membrane lipid polymorphism: relationship to bilayer properties and protein function, in: A.M. Dopico (Ed.), Methods in Membrane Lipids, Humana Press, Totowa, N.J., 2007, pp. 15–26.
[41] A.G. Lee, Lipid–protein interactions in biological membranes: a structural perspective, Biochim. Biophys. Acta 1612 (2003) 1–40.
[42] I.M. Williamson, S.J. Alvis, J.M. East, A.G. Lee, The potassium channel KcsA and its interaction with the lipid bilayer, Cell. Mol. Life Sci. 60 (2003) 1581–1590.
[43] A.G. Lee, How lipids and proteins interact in a membrane: a molecular approach, Mol. Biosyst. 1 (2005) 203–212.
[44] O.S. Andersen, D.B. Sawyer, R.E. Koeppe II, Modulation of channel function by the host bilayer, in: B.P. Gaber, K.R.K. Easwaran (Eds.), Biomembrane structure & function: the state of the art : proceedings of the Indo-U.S. workshop held in January 1991 under the auspices of the Office of the [sic] Naval Research, USA, and the Department of Science and Technology, India, Adenine Press, Schenectady, NY, USA, 1992, pp. 227–244.
[45] J.A. Lundbaek, A.M. Maer, O.S. Andersen, Lipid bilayer electrostatic energy, curvature stress, and assembly of gramicidin channels, Biochemistry USA 36 (1997) 5695–5701.
[46] A.G. Lee, How lipids affect the activities of integral membrane proteins, Biochim. Biophys. Acta, Biomembr. 1666 (2004) 62–87.
[47] O.S. Andersen, R.E. Koeppe II, Bilayer thickness and membrane protein function: an energetic perspective, Annu. Rev. Biophys. Biomol. Struct. 36 (2007) 107–130.
[48] R. Phillips, T. Ursell, P. Wiggins, P. Sens, Emerging roles for lipids in shaping membrane–protein function, Nature 459 (2009) 379–385.
[49] W.G. Wood, U. Igbavboa, W.E. Muller, G.P. Eckert, Cholesterol asymmetry in synaptic plasma membranes, J. Neurochem. 116 (2011) 684–689.
[50] E.K. Esbjorner, P. Lincoln, B. Norden, Counterion-mediated membrane penetration: cationic cell-penetrating peptides overcome Born energy barrier by ion-pairing with phospholipids, Biochim. Biophys. Acta 1768 (2007) 1550–1558.
[51] S. Paula, A.G. Volkov, A.N. Van Hoek, T.H. Haines, D.W. Deamer, Permeation of protons, potassium ions, and small polar molecules through phospholipid bilayers as a function of membrane thickness, Biophys. J. 70 (1996) 339–348.
[52] S. Paula, A.G. Volkov, D.W. Deamer, Permeation of halide anions through phospholipid bilayers occurs by the solubility-diffusion mechanism, Biophys. J. 74 (1998) 319–327.
[53] B.A. Lewis, D.M. Engelman, Lipid bilayer thickness varies linearly with acyl chain-length in fluid phosphatidylcholine vesicles, J. Mol. Biol. 166 (1983) 211–217.
[54] S.E. Feller, K. Gawrisch, Properties of docosahexaenoic-acid-containing lipids and their influence on the function of rhodopsin, Curr. Opin. Struct. Biol. 15 (2005) 416–422.
[55] N. Kucerka, S. Tristram-Nagle, J.F. Nagle, Structure of fully hydrated fluid phase lipid bilayers with monounsaturated chains, J. Membr. Biol. 208 (2005) 193–202.
[56] H. Martinez-Seara, T. Rog, M. Pasenkiewicz-Gierula, I. Vattulainen, M. Karttunen, R. Reigada, Effect of double bond position on lipid bilayer properties: insight through atomistic simulations, J. Phys. Chem. B 111 (2007) 11162–11168.
[57] S. Tristram-Nagle, D.J. Kim, N. Akhunzada, N. Kucerka, J.C. Mathai, J. Katsaras, M. Zeidel, J.F. Nagle, Structure and water permeability of fully hydrated diphytanoylPC, Chem. Phys. Lipids 163 (2010) 630–637.
[58] F.A. Nezil, M. Bloom, Combined influence of cholesterol and synthetic amphiphillic peptides upon bilayer thickness in model membranes, Biophys. J. 61 (1992) 1176–1183.
[59] A.M. Smondyrev, M.L. Berkowitz, Structure of dipalmitoylphosphatidylcholine/cholesterol bilayer at low and high cholesterol concentrations: molecular dynamics simulation, Biophys. J. 77 (1999) 2075–2089.
[60] J.A. Lundbaek, P. Birn, J. Girshman, A.J. Hansen, O.S. Andersen, Membrane stiffness and channel function, Biochemistry USA 35 (1996) 3825–3830.
[61] T.M. Weiss, P.C. van der Wel, J.A. Killian, R.E. Koeppe 2nd, H.W. Huang, Hydrophobic mismatch between helices and lipid bilayers, Biophys. J. 84 (2003) 379–385.
[62] K. Mitra, I. Ubarretxena-Belandia, T. Taguchi, G. Warren, D.M. Engelman, Modulation of the bilayer thickness of exocytic pathway membranes by membrane proteins rather than cholesterol, Proc. Natl. Acad. Sci. U. S. A. 101 (2004) 4083–4088.
[63] S.O. Nielsen, B. Ensing, V. Ortiz, P.B. Moore, M.L. Klein, Lipid bilayer perturbations around a transmembrane nanotube: a coarse grain molecular dynamics study, Biophys. J. 88 (2005) 3822–3828.
[64] A.C. Johansson, E. Lindahl, Protein contents in biological membranes can explain abnormal solvation of charged and polar residues, Proc. Natl. Acad. Sci. U. S. A. 106 (2009) 15684–15689.
[65] F. Yin, J.T. Kindt, Atomistic simulation of hydrophobic matching effects on lipid composition near a helical peptide embedded in mixed-lipid bilayers, J. Phys. Chem. B 114 (2010) 8076–8080.
[66] M.T. Lee, F.Y. Chen, H.W. Huang, Energetics of pore formation induced by membrane active peptides, Biochemistry USA 43 (2004) 3590–3599.
[67] S. Tristram-Nagle, R. Chan, E. Kooijman, P. Uppamoochikkal, W. Qiang, D.P. Weliky, J.F. Nagle, HIV fusion peptide penetrates, disorders, and softens T-cell membrane mimics, J. Mol. Biol. 402 (2010) 139–153.
[68] E. Lindahl, O. Edholm, Mesoscopic undulations and thickness fluctuations in lipid bilayers from molecular dynamics simulations, Biophys. J. 79 (2000) 426–433.
[69] A. Johannsson, G.A. Smith, J.C. Metcalfe, The effect of bilayer thickness on the activity of $(Na^+ + K^+)$-ATPase, Biochim. Biophys. Acta 641 (1981) 416–421.
[70] O. Soubias, S.L. Niu, D.C. Mitchell, K. Gawrisch, Lipid-rhodopsin hydrophobic mismatch alters rhodopsin helical content, J. Am. Chem. Soc. 130 (2008) 12465–12471.
[71] E. Perozo, A. Kloda, D.M. Cortes, B. Martinac, Physical principles underlying the transduction of bilayer deformation forces during mechanosensitive channel gating, Nat. Struct. Biol. 9 (2002) 696–703.
[72] C. Yuan, R.J. O'Connell, P.L. Feinberg-Zadek, L.J. Johnston, S.N. Treistman, Bilayer thickness modulates the conductance of the BK channel in model membranes, Biophys. J. 86 (2004) 3620–3633.
[73] J.R. Elliott, D. Needham, J.P. Dilger, D.A. Haydon, The effects of bilayer thickness and tension on gramicidin single-channel lifetime, Biochim. Biophys. Acta 735 (1983) 95–103.
[74] S. Yamaguchi, T. Hong, A. Waring, R.I. Lehrer, M. Hong, Solid-state NMR investigations of peptide–lipid interaction and orientation of a beta-sheet antimicrobial peptide, protegrin, Biochemistry USA 41 (2002) 9852–9862.
[75] A. Lamaziere, O. Maniti, C. Wolf, O. Lambert, G. Chassaing, G. Trugnan, J. Ayala-Sanmartin, Lipid domain separation, bilayer thickening and pearling induced by the cell penetrating peptide penetratin, Biochim. Biophys. Acta 1798 (2010) 2223–2230.
[76] L. Li, I. Vorobyov, A.D. MacKerell, T.W. Allen, Is arginine charged in a membrane? Biophys. J. 94 (2008) L11–L13.
[77] L.B. Li, I. Vorobyov, T.W. Allen, Potential of mean force and pK(a) profile calculation for a lipid membrane-exposed arginine side chain, J. Phys. Chem. B 112 (2008) 9574–9587.

[78] I. Vorobyov, L.B. Li, T.W. Allen, Assessing atomistic and coarse-grained force fields for protein–lipid interactions: the formidable challenge of an ionizable side chain in a membrane, J. Phys. Chem. B 112 (2008) 9588–9602.
[79] G.M. Torrie, J.P. Valleau, Non-physical sampling distributions in Monte Carlo free-energy estimation—umbrella sampling, J. Comput. Phys. 23 (1977) 187–199.
[80] T. Darden, D. York, L. Pedersen, Particle mesh Ewald—an N.log(N) method for Ewald sums in large systems, J. Chem. Phys. 98 (1993) 10089–10092.
[81] J.P. Ryckaert, G. Ciccotti, H.J.C. Berendsen, Numerical-integration of Cartesian equations of motion of a system with constraints—molecular-dynamics of N-alkanes, J. Comput. Phys. 23 (1977) 327–341.
[82] S.E. Feller, Y.H. Zhang, R.W. Pastor, B.R. Brooks, Constant-pressure molecular-dynamics simulation—the Langevin Piston method, J. Chem. Phys. 103 (1995) 4613–4621.
[83] W.G. Hoover, Canonical dynamics—equilibrium phase-space distributions, Phys. Rev. A 31 (1985) 1695–1697.
[84] S. Nose, A molecular-dynamics method for simulations in the canonical ensemble, Mol. Phys. 52 (1984) 255–268.
[85] J.B. Klauda, R.M. Venable, J.A. Freites, J.W. O'Connor, D.J. Tobias, C. Mondragon-Ramirez, I. Vorobyov, A.D. MacKerell, R.W. Pastor, Update of the CHARMM all-atom additive force field for lipids: validation on six lipid types, J. Phys. Chem. B 114 (2010) 7830–7843.
[86] S.E. Feller, A.D. MacKerell, An improved empirical potential energy function for molecular simulations of phospholipids, J. Phys. Chem. B 104 (2000) 7510–7515.
[87] J.B. Klauda, B.R. Brooks, A.D. MacKerell Jr., R.M. Venable, R.W. Pastor, An ab initio study on the torsional surface of alkanes and its effect on molecular simulations of alkanes and a DPPC bilayer, J. Phys. Chem. B 109 (2005) 5300–5311.
[88] A. Blume, Apparent molar heat-capacities of phospholipids in aqueous dispersion—effects of chain-length and head group-structure, Biochemistry USA 22 (1983) 5436–5442.
[89] S. Kumar, D. Bouzida, R.H. Swendsen, P.A. Kollman, J.M. Rosenberg, The weighted histogram analysis method for free-energy calculations on biomolecules. 1. The method, J. Comput. Chem. 13 (1992) 1011–1021.
[90] I. Vorobyov, T.W. Allen, The electrostatics of solvent and membrane interfaces and the role of electronic polarizability, J. Chem. Phys. 132 (2010) 185101.
[91] A. Aksimentiev, K. Schulten, Imaging alpha-hemolysin with molecular dynamics: ionic conductance, osmotic permeability, and the electrostatic potential map, Biophys. J. 88 (2005) 3745–3761.
[92] W. Humphrey, A. Dalke, K. Schulten, VMD: visual molecular dynamics, J. Mol. Graph. 14 (1996) 33–38.
[93] S. Choe, K.A. Hecht, M. Grabe, A continuum method for determining membrane protein insertion energies and the problem of charged residues (vol 131, pg 563, 2008), J. Gen. Physiol. 134 (2009) 77-77.
[94] G.V. Miloshevsky, A. Hassanein, M.B. Partenskii, P.C. Jordan, Electroelastic coupling between membrane surface fluctuations and membrane-embedded charges: continuum multidielectric treatment, J. Chem. Phys. 132 (2010).
[95] T.W. Allen, O.S. Andersen, B. Roux, On the importance of atomic fluctuations, protein flexibility, and solvent in ion permeation, J. Gen. Physiol. 124 (2004) 679–690.
[96] M. Nina, D. Beglov, B. Roux, Atomic radii for continuum electrostatics calculations based on molecular dynamics free energy simulations, J. Phys. Chem. B 101 (1997) 5239–5248.
[97] A.D. MacKerell, D. Bashford, M. Bellott, R.L. Dunbrack, J.D. Evanseck, M.J. Field, S. Fischer, J. Gao, H. Guo, S. Ha, D. Joseph-McCarthy, L. Kuchnir, K. Kuczera, F.T.K. Lau, C. Mattos, S. Michnick, T. Ngo, D.T. Nguyen, B. Prodhom, W.E. Reiher, B. Roux, M. Schlenkrich, J.C. Smith, R. Stote, J. Straub, M. Watanabe, J. Wiorkiewicz-Kuczera, D. Yin, M. Karplus, All-atom empirical potential for molecular modeling and dynamics studies of proteins, J. Phys. Chem. B 102 (1998) 3586–3616.
[98] R.B. Hermann, Theory of hydrophobic bonding. 2. Correlation of hydrocarbon solubility in water with solvent cavity surface-area, J. Phys. Chem. 76 (1972) 2754–2759.
[99] S. Berneche, M. Nina, B. Roux, Molecular dynamics simulation of melittin in a dimyristoylphosphatidylcholine bilayer membrane, Biophys. J. 75 (1998) 1603–1618.
[100] J. Schamberger, R.J. Clarke, Hydrophobic ion hydration and the magnitude of the dipole potential, Biophys. J. 82 (2002) 3081–3088.
[101] L.G. Wang, P.S. Bose, F.J. Sigworth, Using cryo-EM to measure the dipole potential of a lipid membrane, Proc. Natl. Acad. Sci. U. S. A. 103 (2006) 18528–18533.
[102] N. Kucerka, J.F. Nagle, J.N. Sachs, S.E. Feller, J. Pencer, A. Jackson, J. Katsaras, Lipid bilayer structure determined by the simultaneous analysis of neutron and X-ray scattering data, Biophys. J. 95 (2008) 2356–2367.
[103] E.A. Liberman, V.P. Topaly, Permeability of bimolecular phospholipid membranes for fat-soluble ions, Biofizika 14 (1969) 452–461.
[104] R.F. Flewelling, W.L. Hubbell, The membrane dipole potential in a total membrane-potential model—applications to hydrophobic ion interactions with membranes, Biophys. J. 49 (1986) 541–552.
[105] R.J. Clarke, The dipole potential of phospholipid membranes and methods for its detection, Adv. Colloid Interface Sci. 89 (2001) 263–281.
[106] S.J. Marrink, A.H. de Vries, D.P. Tieleman, Lipids on the move: simulations of membrane pores, domains, stalks and curves, Biochim. Biophys. Acta, Biomembr. 1788 (2009) 149–168.
[107] N. Sapay, D.P. Tieleman, W.F.D. Bennett, Thermodynamics of flip-flop and desorption for a systematic series of phosphatidylcholine lipids, Soft Matter 5 (2009) 3295–3302.
[108] T.W. Allen, O.S. Andersen, B. Roux, Energetics of ion conduction through the gramicidin channel, Proc. Natl. Acad. Sci. U. S. A. 101 (2004) 117–122.
[109] E.V. Schow, J.A. Freites, P. Cheng, A. Bernsel, G. von Heijne, S.H. White, D.J. Tobias, Arginine in membranes: the connection between molecular dynamics simulations and translocon-mediated insertion experiments, J. Membr. Biol. 239 (2011) 35–48.
[110] M. Monne, I. Nilsson, M. Johansson, N. Elmhed, G. von Heijne, Positively and negatively charged residues have different effects on the position in the membrane of a model transmembrane helix, J. Mol. Biol. 284 (1998) 1177–1183.
[111] V.V. Vostrikov, B.A. Hall, D.V. Greathouse, R.E. Koeppe 2nd, M.S. Sansom, Changes in transmembrane helix alignment by arginine residues revealed by solid-state NMR experiments and coarse-grained MD simulations, J. Am. Chem. Soc. 132 (2010) 5803–5811.
[112] A. Finkelstein, Water Movement Through Lipid Bilayers, Pores, and Plasma Membranes: Theory and Reality, Wiley, New York, 1987.
[113] N. Ben-Tal, B. Honig, R.M. Peitzsch, G. Denisov, S. McLaughlin, Binding of small basic peptides to membranes containing acidic lipids: theoretical models and experimental results, Biophys. J. 71 (1996) 561–575.
[114] W.F. Bennett, J.L. MacCallum, D.P. Tieleman, Thermodynamic analysis of the effect of cholesterol on dipalmitoylphosphatidylcholine lipid membranes, J. Am. Chem. Soc. 131 (2009) 1972–1978.
[115] I.V. Vorobyov, V.M. Anisimov, A.D. MacKerell, Polarizable empirical force field for alkanes based on the classical drude oscillator model, J. Phys. Chem. B 109 (2005) 18988–18999.
[116] J.L. Maccallum, W.F. Bennett, D.P. Tieleman, Transfer of arginine into lipid bilayers is nonadditive, Biophys. J. 101 (2011) 110–117.
[117] S.J. Angyal, W.K. Warburton, The basic strengths of methylated guanidines, J. Chem. Soc. (1951) 2492–2494.